Criteria for three-fluid configurations including layers in a pore with nonuniform wettability

M. I. J. van Dijke,[1] M. Piri,[2] J. O. Helland,[3] K. S. Sorbie,[1] M. J. Blunt,[4] and S. M. Skjæveland[5]

Received 22 November 2006; revised 7 August 2007; accepted 28 September 2007; published 11 December 2007.

[1] Recently, a considerable effort has been made to determine the precise displacement criteria for three-fluid configurations in pores of angular cross section. These configurations may contain thick conducting fluid layers, such as oil layers residing between gas in the center and water in the corners of the pore. For pores of uniform, but arbitrary, wettability and in the absence of contact angle hysteresis, a precise thermodynamic criterion for the existence of such layers has been established. In this paper we derive similar criteria for layers in pores of nonuniform wettability, where additional and more complicated layer configurations arise. The criteria for formation and removal of layers are consistent with the capillary entry conditions for the accompanying three-phase bulk displacements, which is essential for accurate pore-scale modeling of three-phase flow. We consider the particular case of three-phase gas invasion in a star-shaped pore with a specific choice of interfacial tensions and contact angles. For this case all possible fluid configurations arise, but only if the water-wet surface in the pore corners is small.

Citation: van Dijke, M. I. J., M. Piri, J. O. Helland, K. S. Sorbie, M. J. Blunt, and S. M. Skjæveland (2007), Criteria for three-fluid configurations including layers in a pore with nonuniform wettability, *Water Resour. Res.*, *43*, W12S05, doi:10.1029/2006WR005761.

1. Introduction

[2] Pore-scale network modeling of multiphase flow, say water, oil or nonaqueous phase liquid (NAPL) and gas (air), crucially depends on the entry conditions for displacement events in individual pores. For two-phase flow in pores with noncircular cross section, entry pressures for bulk displacements, in the presence of wetting films, can be calculated using the Mayer, Stowe and Princen (MS-P) theory [*Mayer and Stowe*, 1965; *Princen*, 1969a, 1969b, 1970]. Later developments have been summarized by *Lago and Araujo* [2001]. *van Dijke and Sorbie* [2003] have extended this theory, which is based on minimization of the free energy, to three-phase capillary entry pressures.

[3] Additionally, in three-phase flow layers of the intermediate-wetting phase may form, sandwiched between the nonwetting bulk phase in the pore center and the wetting phase in the pore corner, for example oil layers between bulk gas and water in the corners in a water-wet medium. These layers may significantly enhance the relative permeability of the layer phase. It is often the case that the flow of oil during gas injection processes is controlled, at oil saturations smaller than the water flood residual oil saturation, by drainage of oil through the layers. This means that stability and conductance of the layers are the main factors that determine how quickly the oil relative permeability may decrease during a gas injection process, which obviously controls the residual oil saturation and rate of oil recovery [*Sahni et al.*, 1998; *DiCarlo et al.*, 2000; *Dong and Chatzis*, 2003].

[4] *van Dijke et al.* [2004] have shown that the phase pressure combinations associated with displacements of the intermediate-wetting phase layers can also be calculated using the (extended) MS-P theory. As a result, for a pore of given shape and (uniform) arbitrary wettability, the space of three-phase pressure combinations is uniquely delineated with respect to the possible pore cross-sectional fluid occupancies, where the separations are given by the entry conditions related to either bulk or layer displacements [*van Dijke and Sorbie*, 2007]. Using a capillary bundle model, *van Dijke and Sorbie* [2007] showed that implementation of these criteria may have a major effect on the simulation of three-phase displacements processes, such as NAPL migration in the unsaturated zone and gas injection for improved oil recovery.

[5] A further complication arises in pores, which have undergone a wettability change after primary drainage [*Kovscek et al.*, 1993]. Combining the MS-P theory for two-phase displacements in these nonuniformly wetted pores [*Ma et al.*, 1996; *Blunt*, 1997], and the three-phase capillary entry pressures in uniformly wetted pores [*van Dijke and Sorbie*, 2003; *van Dijke et al.*, 2004], *Piri and Blunt* [2004] and *Helland and Skjæveland* [2006] calculated

[1]Institute of Petroleum Engineering, Heriot-Watt University, Edinburgh, UK.
[2]Department of Chemical and Petroleum Engineering, University of Wyoming, Laramie, Wyoming, USA.
[3]International Research Institute of Stavanger, Stavanger, Norway.
[4]Department of Earth Science and Engineering, Imperial College, London, UK.
[5]Department of Petroleum Engineering, University of Stavanger, Stavanger, Norway.

0043-1397/07/2006WR005761$09.00

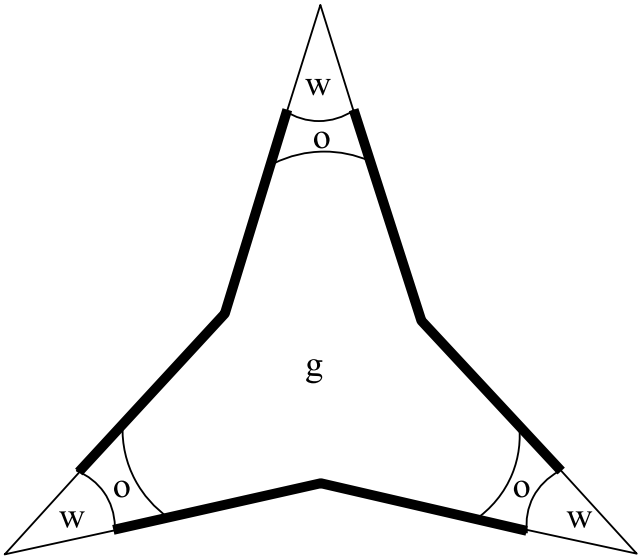

Figure 1. Cross section of a star-shaped pore with water wetting layers in the corners, gas in the center, and oil layers in between. Bold lines indicate surfaces of altered wettability.

two-phase and three-phase capillary entry pressures for piston-like displacements in nonuniformly wetted pores. The stability of layers arising during these displacements was assessed using a geometrical layer collapse criterion [*Hui and Blunt*, 2000]. *Helland and Skjæveland* [2006] implemented the entry conditions for nonuniformly wetted pores in a capillary bundle model, for which they derived a set of three-phase capillary pressure-saturation curves. They found that the pore occupancies and the saturation dependencies of the three-phase capillary pressures (hence the three-phase relative permeabilities) during gas invasion after water flooding, varied with the wettability changes after primary drainage. In fact, pore occupancies and displacement orders were derived that can never occur for a bundle of uniformly wetted pores, even when the proper three-phase entry criteria are implemented [*van Dijke and Sorbie*, 2007].

[6] As a preliminary to the present paper, *van Dijke and Sorbie* [2006] recently derived the thermodynamic criteria for displacements involving an oil layer sandwiched between water in the center and in the corners of a nonuniformly wetted pore during a two-phase water flood. Entry conditions for nonuniformly wetted pores have successfully been implemented in two-phase pore-scale network models [e.g., *Øren et al.*, 1998; *Patzek*, 2001; *Valvatne and Blunt*, 2004], although without the thermodynamic criterion for the formation and removal of oil layers. Instead the geometrical layer collapse criterion [*Hui and Blunt*, 2000] was used.

[7] In existing three-phase pore-scale network models with (nonuniformly wetted) angular pores [e.g., *Fenwick and Blunt*, 1998; *Lerdahl et al.*, 2000; *Piri and Blunt*, 2005a] only the two-phase capillary entry pressures have been used, even for displacements involving all three phases. Geometrical collapse criteria were employed [*Fenwick and Blunt*, 1998; *Hui and Blunt*, 2000; *Piri and Blunt*, 2004] to assess the existence of these layers. There are actually three mechanisms by which layers of the intermediate-wetting phase may arise in three-phase systems and we describe these for a water-wet system with oil as the intermediate-wetting phase. First, the layers may form by bulk gas invasion into bulk oil, which may leave behind some of the oil, residing in layers between bulk gas and water in the corners [*DiCarlo et al.*, 2000]. Second, oil layers may form as a result of oil invasion into a pore with bulk gas and water in the corners [e.g., *Øren et al.*, 1992]. This is one of the main mechanisms that allow recovery of water flood residual oil by gas injection. Third, oil layers may move alongside bulk gas during gas invasion into a water-filled pore. Evidence of this scenario is clear from micromodel experiments [*Dong et al.*, 1995; *Grattoni et al.*, 1997; *Keller et al.*, 1997; *Sohrabi et al.*, 2004]. Most existing three-phase pore-scale network models only include the first mechanism, while *Piri and Blunt* [2005a, 2005b] model the first two layer formation scenarios. They consider layer formation or collapse as a separate displacement event based on the geometrical criteria. However, none of the mentioned three-phase network models has considered the third mechanism, i.e., a displacement event by which a water-filled pore changes to a configuration with bulk gas, oil in layers and water in the corners. This displacement event is discussed in the present paper, alongside the remaining mechanisms, all based on the corresponding full thermodynamic criteria, i.e., MS-P theory, although the geometrical criteria continue to play a role.

[8] In summary, the main purpose of this paper is to derive the proper three-phase flow thermodynamic criteria for the existence of fluid layers in a nonuniformly wetted pore and to demonstrate how these fit in with the capillary entry pressures for the corresponding bulk displacements. Rather than deriving an abstract general theory, we choose a specific range of contact angles and the related phase wetting order, as well as a specific pore geometry, and we discuss the arising fluid configurations and displacements with their entry conditions. This example is general enough to be extended straightforwardly to other cases.

2. Model

2.1. Displacement Scenarios and Pore Fluid Configurations

[9] As a model pore, we consider a straight tube with a cross section shaped as a regular three-cornered star, with corner half angle $\gamma \leq \pi/6$, as shown in Figure 1. After primary drainage (oil invasion into the water-filled water-wet pore) the surface in the center of the pore, which was contacted by oil, has become more oil-wet than the corners of the pore, where water remains. As an example, Figure 1 shows the possible situation after an increase of the water pressure, followed by gas invasion. The latter has displaced most of the oil in the center, leaving oil layers behind. Below, we describe the possible displacement scenarios during gas invasion into the different pore fluid occupancies resulting from a water flood following primary drainage.

[10] The maximum oil-water pressure difference P_{ow}^{dr}, with $P_{ij} = P_i - P_j$, reached at the end of the primary drainage process determines the length of contact L_s^{dr} (between water and solid) of the corner surface that does not change wettability. Drainage has taken place at a contact angle θ_{ow}^{dr} (taken as 0). P_{ow}^{dr} is usually larger than the MS-P oil-water capillary entry pressure P_{ow}^{MSP}, for which equation (A9) provides an explicit expression. For processes following

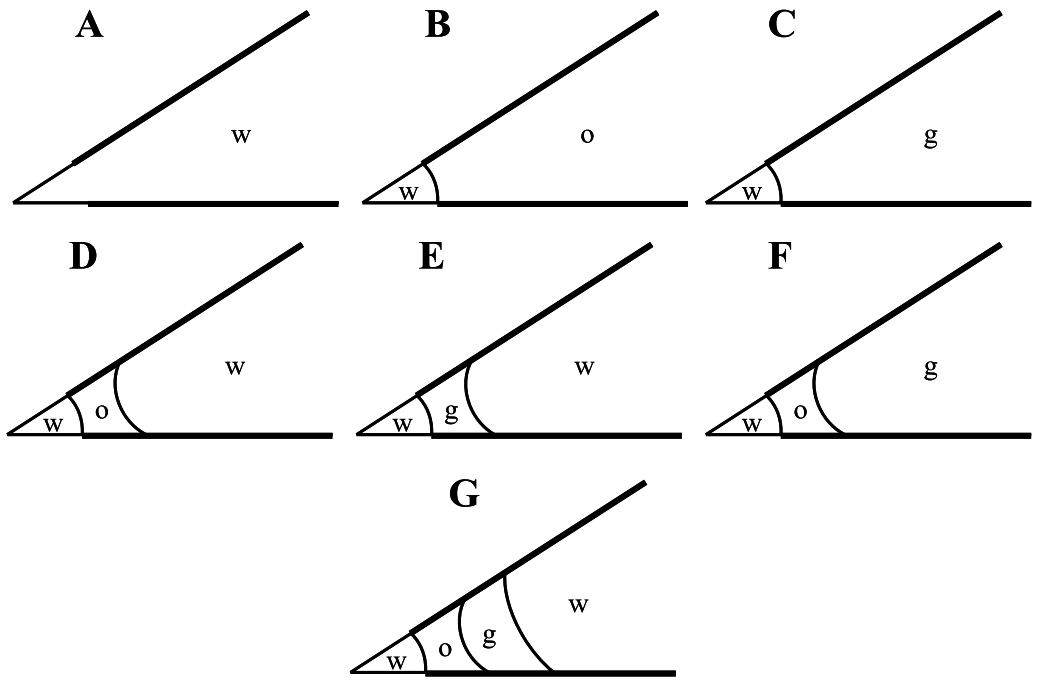

Figure 2. Occupancies in corners of a regular star for fluid configurations associated with three-phase gas invasion, when gas is wetting to water on the surface of altered wettability (bold lines). Occupancy F corresponds to the fluid configuration of Figure 1.

drainage, we define at the water-wet (unaltered) surface receding and advancing oil-water contact angles $\theta^w_{ow,r}$ and $\theta^w_{ow,a}$. On the oil-wet (altered) surface in the center of the pore we define $\theta^o_{ow,r}$ and $\theta^o_{ow,a}$.

[11] A water flood following primary drainage may lead to pore fluid configurations B, D or A, for which the corner occupancies are sketched in Figure 2 for subsequently larger water pressures. More precisely, water invasion in configuration B may either lead directly to configuration A (B→A) and the entry condition for the corresponding bulk displacement is given by *Ma et al.* [1996] or a bulk displacement from B to D followed by a layer displacement from D to A may occur (B→D→A) [*Piri and Blunt*, 2004; *van Dijke and Sorbie*, 2006]. The relevant contact angles during water invasion are $\theta^w_{ow,a}$ and $\theta^o_{ow,a}$, where the (outer) oil-water arc meniscus (ow AM) in the corners is pinned at the contact length L_s^{dr} with the hinging angle $\theta_{ow,h}$ satisfying $\theta^w_{ow,a} < \theta_{ow,h} < \theta^o_{ow,a}$. We assume that $\theta^o_{ow,a}$ is large enough to prevent configurations B and D with the outer AM in a stable position on the oil-wet surface. In fact, presence of the inner AM in configuration D requires $\theta^o_{ow,a} > \pi/2 + \gamma$.

[12] Gas invasion into configurations A, B and D may then lead to the remaining configurations sketched in Figure 2 as part of the series of displacements indicated below, if we assume that gas is wetting to water on the oil-wet surface, i.e., the gas-water contact angles $\theta^o_{gw,r}$ and $\theta^o_{gw,a}$ are larger than $\pi/2$. During gas invasion the relevant gas-water angles are the receding angles $\theta^w_{gw,r}$ and $\theta^o_{gw,r}$, for which we assume $\theta^o_{gw,r} > \pi/2 + \gamma$ and $\theta^w_{gw,r} < \theta^o_{gw,r}$. The former condition allows presence of the (inner) gw AM on the oil-wet surface, for example in configuration E. The latter condition may cause the outer gw AM to be pinned with hinging angle $\theta_{gw,h}$ satisfying $\theta^w_{gw,r} < \theta_{gw,h} < \theta^o_{gw,r}$. Similarly, we use receding gas-oil contact angles $\theta^w_{go,r}$ and $\theta^o_{go,r}$ with $\theta^o_{go,r} < \pi/2 - \gamma$, to allow the presence of the go AM on the oil-wet surface and $\theta^w_{go,r} > \theta^o_{go,r}$. During gas invasion the oil-water contact angles are taken from the preceding water flood.

[13] In general, between the seven configurations sketched in Figure 2, twenty-one displacements are possible. The prescription that gas is invading, by increasing the gas pressure and fixing the oil-water pressure difference, determines the direction in which the displacements are taking place (e.g., A→E, rather than E→A), because in principle the gas volume should increase. Additionally, we assume that gas invasion does not lead to bulk phase invasion of oil or water, specifically displacements B→E and B→G, as this would require a definite change of the oil-water pressure difference. Starting with occupancies following a water flood (A, B and D), the displacements A→C, A→E, A→F, A→G, B→C, B→F, D→C, D→E, D→F and D→G may occur. Notice, that we allow for invasion of a second phase accompanying the invading gas, specifically an oil layer as in displacements A→F and A→G, which is well possible when in a porous medium oil is available in neighboring pores. Since gas injection into occupancy C cannot lead to qualitatively different occupancies, for a sufficiently high gas pressure occupancy C is the final stage for gas invasion. However, for an increasing gas pressure further displacements from the remaining occupancies E, F and G are possible, i.e., E→C, E→F, F→C, G→C, G→E and G→F. This makes a total of 16 possible displacements. Depending on the specific conditions series of displacements may occur, such as A→E→C or D→G→F→C.

[14] Displacements A→C, B→C, B→F, D→C, D→F, E→C and G→F involving a change of bulk phase from

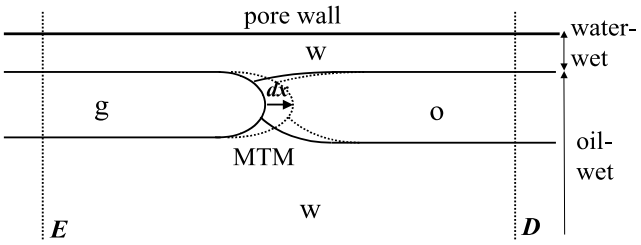

Figure 3. Slice along the pore through one of the corners for a small movement *dx* of the main terminal meniscus (MTM) associated with displacement D→E. The dotted lines indicate the locations of the two cross sections shown in Figure 2.

water (or oil) to gas have been analyzed in detail by *Piri and Blunt* [2004] and *Helland and Skjæveland* [2006]. Displacement A → E is a two-phase layer displacement, analyzed by *van Dijke and Sorbie* [2006]. However, the remaining displacements have not been studied before, as they all involve formation or removal of fluid layers during a three-phase displacement, although the transitions F→C and G→E have been considered based on a geometrical layer collapse criterion. Consequently, although configurations E and G were anticipated before, they could not be produced during gas invasion using bulk displacement and layer collapse mechanisms only.

[15] Obviously, higher-order invasion processes, which may occur during water-alternating-gas injection in oil recovery or during fluctuation of the groundwater table around a NAPL spill, may lead to configurations additional to those sketched in Figure 2. These configurations are the result of further hysteresis in the prevailing contact angles [*Piri and Blunt*, 2004; *Helland and Skjæveland*, 2006], but the method of calculating the corresponding displacement criteria is the same as that outlined below.

2.2. Free Energy Balance

[16] In general, the capillary entry pressures and layer displacement criteria are calculated from minimization of the Helmholtz free energy F for a small displacement dx of the fluids along the pore, where one cross-sectional configuration displaces another. The three-phase pressure combination for which $dF = 0$ represents the minimum free energy state [*Firoozabadi*, 1999] and it constitutes the criterion for the equilibrium or quasi-static displacement in the pore.

[17] In Figure 3, a slice along the pore, through one corner, is shown for displacement D→E. The cross-sectional configurations meet at the main terminal meniscus (MTM), which may consist of several fluid-fluid interfaces separated by contact lines. For example, in Figure 3, go, gw and ow interfaces can be found at the MTM. The precise shapes of the interfaces at the MTM are unknown, but this does not affect the analysis below, as only the corresponding effective radii of curvature r_{ij} ($ij = gw, go, ow$) are important. These effective radii are defined through the pressure differences and the interfacial tensions σ_{ij} as

$$P_{ij} = \frac{\sigma_{ij}}{r_{ij}} \tag{1}$$

and related to each other through $P_{gw} = P_{go} + P_{ow}$. Far away from the MTM the interfaces between the various fluids, i.e., the AMs, can be assumed cylindrical and their effective radii are identical to their single finite radii of curvature. At equilibrium the respective effective radii at the MTM and at the AMs must be the same and they are fixed during the displacement. Furthermore, at the MTM the interfaces assume contact angles θ_{ij}^{MTM} with the pore wall that are either receding or advancing, depending on the direction of the considered displacement, but not hinging. Therefore, if the corresponding AM contact angles hinge, then these are different from the MTM angles.

[18] The general equation for the variation of Helmholtz free energy dF corresponding to an arbitrary three-phase displacement in a pore is [*van Dijke et al.*, 2004; *Piri and Blunt*, 2004]

$$\begin{aligned} dF = {} & P_{gw}dV_w + P_{go}dV_o + \sigma_{gw}\left(dA_{gw} - \cos\theta_{gw}^{MTM}dA_{ws}\right) \\ & + \sigma_{go}\left(dA_{go} - \cos\theta_{go}^{MTM}dA_{os}\right) + \sigma_{ow}dA_{ow}, \end{aligned} \tag{2}$$

where dV_I denotes the change of volume of phase i, dA_{is} denotes the change of the fluid-solid contact area for phases i, and dA_{ij} denotes the change of the fluid-fluid contact area between phases i and j. For each specific displacement, expressions for these volume and area changes need to be determined, as illustrated below. Equation (2) also contains the MTM contact angles θ_{gw}^{MTM} and θ_{go}^{MTM}, where the third possible contact angle θ_{ow}^{MTM} follows from the Bartell-Osterhof equation

$$\sigma_{gw}\cos\theta_{gw} = \sigma_{go}\cos\theta_{go} + \sigma_{ow}\cos\theta_{ow}, \tag{3}$$

applied to the MTM angles. By solving the equation $dF = 0$ and using equation (1), a functional relation between two of the effective radii of curvature r_{ij} is obtained, which corresponds to the minimum free energy pressure combination at which the considered quasi-static displacement occurs [*van Dijke and Sorbie*, 2003].

[19] As an example, we give the expressions for the volume and area changes related to the layer displacement D → E shown in Figure 3, i.e.,

$$\begin{aligned} dV_w = {} & \left\{-3\left(A^{(\alpha)}\left(r_{wg}, \theta_{wg}^{AM2}\right) - A^{(\alpha)}\left(r_{wo}, \theta_{wo}^{AM2}\right)\right)\right. \\ & \left. - 3\left(A^{(\alpha)}\left(r_{ow}, \theta_{ow}^{AM1}\right) - A^{(\alpha)}\left(r_{gw}, \theta_{gw}^{AM1}\right)\right)\right\}dx \\ dV_o = {} & -3\left(A^{(\alpha)}\left(r_{wo}, \theta_{wo}^{AM2}\right) - A^{(\alpha)}\left(r_{ow}, \theta_{ow}^{AM1}\right)\right)dx \end{aligned} \tag{4a}$$

$$\begin{aligned} dA_{ws} = {} & \left\{-3\left(L_s^{(\alpha)}\left(r_{wg}, \theta_{wg}^{AM2}\right) - L_s^{(\alpha)}\left(r_{wo}, \theta_{wo}^{AM2}\right)\right)\right. \\ & \left. -3\left(L_s^{(\alpha)}\left(r_{ow}, \theta_{ow}^{AM1}\right) - L_s^{(\alpha)}\left(r_{gw}, \theta_{gw}^{AM1}\right)\right)\right\}dx, \\ dA_{os} = {} & -3\left(L_s^{(\alpha)}\left(r_{wo}, \theta_{wo}^{AM2}\right) - L_s^{dr}\right)dx \end{aligned} \tag{4b}$$

$$\begin{aligned} dA_{gw} = {} & 3L_f^{(\alpha)}\left(r_{wg}, \theta_{wg}^{AM2}\right) + 3L_f^{(\alpha)}\left(r_{gw}, \theta_{gw}^{AM1}\right)dx, \\ dA_{go} = {} & 0, \\ dA_{ow} = {} & -3\left(L_f^{(\alpha)}\left(r_{wo}, \theta_{wo}^{AM2}\right) + L_f^{(\alpha)}\left(r_{ow}, \theta_{ow}^{AM1}\right)\right)dx \end{aligned} \tag{4c}$$

where the geometrical functions $A^{(\alpha)}(r_{ij}, \theta_{ij})$, $L_s^{(\alpha)}(r_{ij}, \theta_{ij})$, $L_f^{(\alpha)}(r_{ij}, \theta_{ij})$ arising in a corner α are explained in Appendix A. The superscripts AM1 and AM2 refer to the outer and inner arc menisci in the corners respectively, as explained in Figure A1. We solve equation (2) for r_{gw} as a function of r_{ow}. Since AM2 arises on the oil-wet surface, $\theta_{wo}^{AM2} = \pi - \theta_{ow,a}^{o}$, which is taken from the preceding water flood and $\theta_{wg}^{AM2} = \pi - \theta_{gw,r}^{o}$.

[20] For this displacement at least the ow AM1 is pinned at the contact length L_s^{dr}, with the hinging angle $\theta_{ow}^{AM1} = \theta_{ow,h}$. Assuming that L_s^{dr} is known from the primary drainage process and r_{ow} from the end of the preceding water flood, $\theta_{ow,h}$ follows from equation (A1b), with $L_s^{dr} = L_s^{(\alpha)}(r_{ow}, \theta_{ow,h})$. Similarly, the gw AM1 may be pinned, but in this case r_{gw} and $\theta_{gw,h}$ are both unknown. Therefore we take equation (A1b) as an additional constraint, i.e.

$$L_s^{dr} = 2r_{gw}\frac{\cos(\theta_{gw,h} + \gamma)}{\sin\gamma} \quad \text{for} \quad \theta_{gw,r}^{w} < \theta_{gw,h} < \theta_{gw,r}^{o} \tag{5}$$

At the MTM the contact angles in equation (2) are $\theta_{go}^{MTM} = \theta_{go,r}^{o}$ and $\theta_{gw}^{MTM} = \theta_{gw,r}^{o}$.

[21] However, it is not a priori known that the gw AM1 is actually pinned as it could also be present on the water-wet surface. In this case, the term $\cos\theta_{gw}^{MTM}\, dA_{ws}$ in equation (2) should be split as $\cos\theta_{gw}^{MTM}\, dA_{ws} = \cos\theta_{gw,r}^{w}\, dA_{ws}^{w} + \cos\theta_{gw,r}^{o}\, dA_{ws}^{o}$, with

$$dA_{ws}^{w} = -3\left(L_s^{dr} - L_s^{(\alpha)}\left(r_{gw}, \theta_{gw}^{AM1}\right)\right)dx \tag{6a}$$

$$dA_{ws}^{o} = \left\{-3\left(L_s^{(\alpha)}\left(r_{wg}, \theta_{wg}^{AM2}\right) - L_s^{(\alpha)}\left(r_{wo}, \theta_{wo}^{AM2}\right)\right) - 3\left(L_s^{(\alpha)}\left(r_{ow}, \theta_{ow}^{AM1}\right) - L_s^{dr}\right)\right\}dx \tag{6b}$$

Additionally, for the gw AM1 the appropriate contact angle would be $\theta_{gw}^{AM1} = \theta_{gw,r}^{w}$.

[22] It follows easily that for displacement D→E AM1 does not enter the water-wet surface with the present choice of contact angles. Basically, the wo and wg AM2 on the oil-wet surfaces, which constitute configurations D and E, can exist only for negative P_{ow} and P_{gw} respectively, whereas the possible presence of the AM1 on the water-wet surfaces requires positive pressure differences. However, for other displacements the gw AM1 may enter the water-wet surface, for example for displacement F→C.

[23] For completeness, we also give the expressions for the volume and area changes in equation (2) related to a bulk displacement, for example for G→F, which involve the total cross-sectional area A and perimeter L_s

$$dV_w = -\left(A - 3A^{(\alpha)}\left(r_{wg}, \theta_{wg}^{AM2}\right)\right)dx, \quad dV_o = 0 \tag{7a}$$

$$dA_{ws} = -\left(L_s - 3L_s^{(\alpha)}\left(r_{wg}, \theta_{wg}^{AM2}\right)\right)dx, \quad dA_{os} = 0 \tag{7b}$$

$$dA_{gw} = 3L_f^{(\alpha)}\left(r_{wg}, \theta_{wg}^{AM2}\right)dx, \quad dA_{go} = 0, \quad dA_{ow} = 0 \tag{7c}$$

It follows that the expression for dF in equation (2) reduces to the two-phase expression in equation (A8) with $ij = gw$. Moreover, because only AM2 is involved, for which the contact angle does not hinge and is the same as the MTM angle, i.e., $\theta_{wg}^{AM2} = \theta_{wg}^{MTM} = \pi - \theta_{gw}^{MTM}$, G→F represents a "classical" two-phase MS-P displacement. For this displacement an explicit solution for the capillary entry pressure, $P_{gw}^{MSP} = -P_{wg}^{MSP}$, in this case independent of P_{ow}, is available, given by equation (A9) with $ij = wg$. Furthermore, the same expressions are found for displacement E→C. Similarly, identical expressions arise for displacements G→E and F→C.

[24] Also for some of the other displacements occurring during gas invasion explicit solutions are available. B→F is also a classical two-phase displacement occurring entirely on the oil-wet surface, whereas D→F is a bulk displacement (of water by gas) affected by the pressure of the third phase (oil) [*van Dijke and Sorbie*, 2003]. Displacement D→G represents layer invasion on the oil-wet surface [*van Dijke et al.*, 2004].

2.3. Computational Procedure

[25] For primary drainage the explicit solution for the capillary entry pressure P_{ow}^{MSP} is given by equation (A9). For the water flood displacements B→A, B→D and D→A, the two-phase expression for dF of equation (A8) applies. For displacement B→D the explicit solution (A9) is again found. However, for the remaining displacements a simple Newton-Raphson method is used to determine the zeros of dF, i.e., values of r_{ow} and the accompanying value of $\theta_{ow,h}$ when relevant [e.g., *van Dijke and Sorbie*, 2006]. For gas invasion, we calculate for a series of r_{ow} (with $\theta_{ow,h}$) resulting from the water flood, solutions of $dF = 0$, also using a Newton-Raphson method, where equation (5) is used to determine the possible hinging angles. Because it is not always certain whether the gw AM1 is actually pinned, as discussed above, we calculate a threshold value r_{gw}^{*} from equation (5), i.e., $L_s^{dr} = L_s^{(\alpha)}(r_{gw}^{*}, \theta_{gw,r}^{w})$, at which AM1 is about to enter the water-wet surface. Then, we take $\theta_{gw}^{AM1} = \theta_{gw,r}^{w}$ if $r_{gw} < r_{gw}^{*}$ and calculate $\theta_{gw}^{AM1} = \theta_{gw,h}$ from equation (5) if $r_{gw} > r_{gw}^{*}$.

[26] Since for most displacements two solutions arise, we carefully check if the obtained solutions are geometrically possible. Usually, one of the two solutions is ruled out as it involves a radius of curvature for one or more of the AMs that is larger than the corresponding snap-off value, for which the corresponding pressure criteria are presented in Appendix A. Furthermore, for configurations involving layers, we check if the geometrical collapse criteria have not been violated. These criteria simply state that the AMs surrounding a layer should not touch and they are derived from geometrical expressions for the contact lengths as given in Appendix A.

3. Results and Discussion

[27] We have calculated the entry pressures related to all 16 displacements that may arise during gas invasion using the following parameters: interfacial tensions are $\sigma_{gw} = 30$ mN/m, $\sigma_{go} = 10$ mN/m, $\sigma_{ow} = 28$ mN/m; relevant contact angles are $\theta_{ow,a}^{w} = 0.760$, $\theta_{ow,a}^{o} = 3.14$, $\theta_{gw,r}^{w} = 0.182$, $\theta_{gw,r}^{o} = 2.22$, $\theta_{go,r}^{w} = 0.400$ and $\theta_{go,r}^{o} = 0.200$. Notice that the triple of contact angles for the water-wet contact

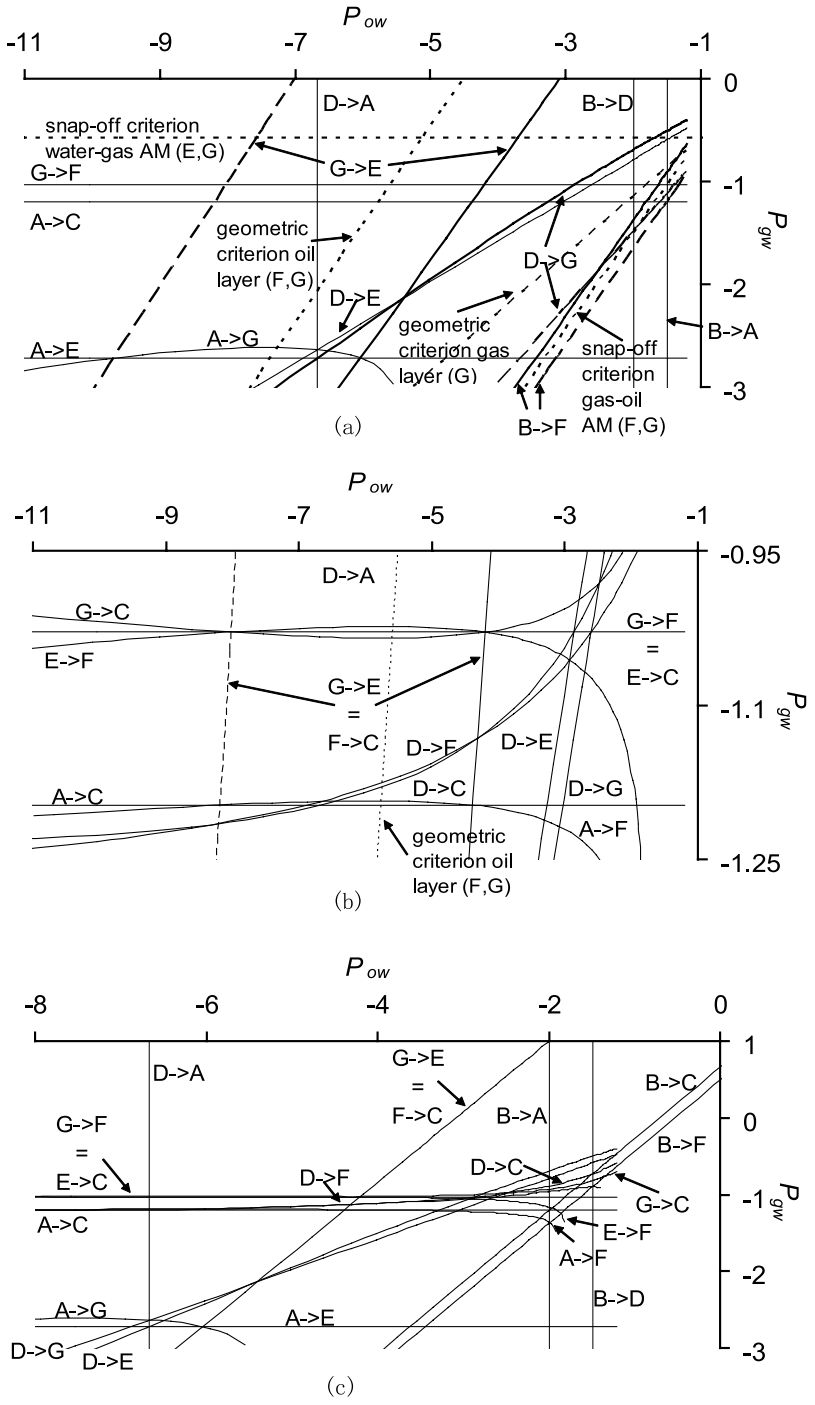

Figure 4. Capillary entry pressures and layer displacement criteria in terms of P_{gw} versus P_{ow} for gas invasion when $P_{ow}^{MSP}/P_{ow}^{dr} = 0.1$. Vertical lines indicate criteria for the preceding water flood. Additionally, geometrical layer and snap-off criteria are indicated as dotted lines in Figures 4a and 4b. The dashed lines indicate displacement criteria that are excluded for geometrical reasons. Figure 4b is a close-up of Figure 4a by stretching the vertical axis. Figure 4c shows all the geometrically allowed solutions for the displacements.

surfaces satisfies the Bartell-Osterhof equation (3) and so does the triple of angles for the oil-wet surfaces. A small corner angle of $\gamma = \pi/24 \approx 0.131$ is used. The entry pressures are determined for four different maximum drainage oil-water pressures relative to the MS-P capillary entry pressure, i.e., $P_{ow}^{MSP}/P_{ow}^{dr} = 0.1$, $P_{ow}^{MSP}/P_{ow}^{dr} = 0.3$, $P_{ow}^{MSP}/P_{ow}^{dr} = 0.5$ and $P_{ow}^{MSP}/P_{ow}^{dr} = 1$, where these ratios are proportional to the contact lengths L_s^{dr} of the remaining water-wet surface.

[28] In Figure 4, capillary entry pressures and thermodynamic layer displacement criteria based on equation (2) are presented in terms of the gas-water pressure differences P_{gw} versus the oil-water pressure differences P_{ow} for $P_{ow}^{MSP}/P_{ow}^{dr} = 0.1$. Additionally, the geometrical criteria for the gas layer in

configuration G and the oil layer in configurations F and G, as well as the snap-off criteria for the water-gas and gas-oil AM2 are included in Figures 4a and 4b. The pressure differences have been normalized through multiplication by r_{in}/σ_{ij}, making these identical to the normalized curvatures of the corresponding interfaces.

[29] With Figure 4a we demonstrate first how the geometrical criteria, including snap-off, restrict the existence of the configurations with layers, E, F and G, as well as the corresponding displacements. For the oil layer removal displacement G→E two possible solutions arise as indicated in Figure 4. However, the geometrical layer criterion for the oil layer in configuration G (and configuration F), given by equation (A6) excludes the larger solution. Similarly, two solutions for the gas layer invasion displacement D→G arise, of which the lower is excluded by the criterion for the gas layer in configuration G, given by equation (A7). For the bulk gas displacement B→F, leading to the formation of an oil layer, the lower solution is excluded based on the snap-off criterion for the gas-oil AM in configuration F, given by equation (A4). If we also include the snap-off criterion for the water-gas AM2, we find that the pressure combinations where configuration G is allowed, based on geometrical criteria alone, are very limited indeed. It follows similarly that the pressure combinations for which configuration F can exist is also limited, but less restricted than for configuration G. The geometrical criterion for the gas layer in configuration E, given by equation (A5), is approximately $P_{gw}^{geom} = -7.00$, which is not very restrictive compared to other criteria. We have used the corresponding criteria for all other displacements to find the unique geometrically possible solution.

[30] Figure 4a already reveals some of the consistent crossovers of the displacement criteria. For example, the criteria for displacements A→E, A→G and G→E intersect (twice), in exactly the same point. As demonstrated by *van Dijke and Sorbie* [2007], this indicates that around these crossovers the free energies of the corresponding occupancies (A, G and E) are ordered, such that there is a unique relation between these occupancies and the three-phase pressure combinations, here the pressure differences (P_{ow}, P_{gw}). This consistency is a direct consequence of the Bartell-Osterhof equation (3). In Figure 4b, solutions have been added that show up close to those relating to displacements A→C and G→F, showing all the corresponding consistent crossovers. Observe that consistent intersections of four criteria occur (twice) for displacements E→F, G→C, G→E and G→F. Because of the geometric layer criterion for the oil layer in configurations F and G, the solutions and corresponding crossovers to the left of the criterion (lower P_{ow}) are no longer relevant.

[31] In Figure 4c all displacement criteria corresponding to configurations that are geometrically allowed are presented. We mainly consider negative values of P_{ow}, since all the water-flood displacements (B→A, B→D and D→A) have occurred for negative P_{ow}. All three-phase entry pressures have negative P_{gw}, apart from those associated with displacements B→C, B→F and G→E (F→C), for large P_{ow}. The latter means that, only for these displacements, the (hinging) contact angle at the outer gw AM1 θ_{gw}^{AM1} in configurations E (or C) is smaller than $\pi/2$, which is perfectly reasonable for configuration C. For even larger P_{gw} the gw AM1 may enter the water-wet surface, as discussed in section 2.2.

[32] Next, we work out which entry pressures and crossovers are actually relevant during gas invasion following a water flood. The vertical lines represent the water flood entry pressures. A water flood, in which P_{ow} decreases, starting with configuration B at large P_{ow} will first lead to configuration D, at B→D and subsequently to configuration A at D→A rendering B→A irrelevant. The geometrical criterion for the oil layer, given by equation (A5) is approximately $P_{ow}^{geom} = -12.3$, which is far less restrictive than the thermodynamic criterion for displacement D→A at $P_{ow} = -6.67$ [*van Dijke and Sorbie*, 2007], below which configuration D can no longer exist.

[33] Gas invasion is represented by increasing P_{gw}, starting from a very small value, at a constant P_{ow}. For example at $P_{ow} = -4$ the two-phase oil water configuration is D, hence during increase of P_{gw} the displacement "away from D" with the lowest entry pressure is D→G. Having arrived at G, the lowest entry pressure "away from G" is G→F. Finally, the lowest entry pressure "away from F" is F→C (i.e., G→E). In effect, we have found the displacement series D→G→F→C. Similarly, if we start at $P_{ow} = -1$ the two-phase oil water configuration is B. In the corresponding regime, which also extends to positive P_{ow}, the lowest entry pressure displacement "away from B" is B→F, followed by F→C (at positive P_{gw}), yielding B→F→C. If we start at $P_{ow} = -7$, the two-phase oil water configuration is A and the series A→E→C is found. For a very low oil-water pressure, say $P_{ow} = -11$, Figures 4a and 4b suggest that the series A→G→F→C results, but because configurations F and G are geometrically disallowed, the first allowed solution greater than A→G, i.e., A→E, prevails, followed again by E→C (rather than E→F). This process of finding the lowest entry pressures can be formalized using the ordering of the free energies for all possible pairs of fluid configurations [*van Dijke and Sorbie*, 2007]. It may be clear that the (relevant) consistent crossovers delineate the pressure space with respect to the different possible displacement series.

[34] After examination of all possible displacement paths between the various crossovers, we present in Figure 5a the delineation of the (P_{ow}, P_{gw}) space with respect to the different configurations of Figure 2. Entry conditions that are not relevant for any pressure combination, such as B→C have been removed. Notice the various remaining relevant crossovers, which all separate 3 configurations, except the crossover of 4 solutions, which separates 4 configurations (C, E, F and G), although two of the solutions (E→F and G→C) are not relevant at all. Figure 5a reveals that transition between configurations G to C is mediated by either configuration E (for lower P_{ow}) or by configuration F (for higher P_{ow}), whereas a direct transition from G→C only takes place at the crossover.

[35] We conclude that for this high $P_{ow}^{dr} = 10P_{ow}^{MSP}$, where there is only a small water-wet surface and little water left in the pore corners, (in combination with the small corner half angle) a complicated set of entry pressures arises, in which all 7 possible configurations of Figure 2 occur. In particular, configurations E and G are present, although they are only intermediate configurations during a gas invasion process. Notice also that the existence of configuration G, with both a gas and an oil layer, is limited by the layer displacements

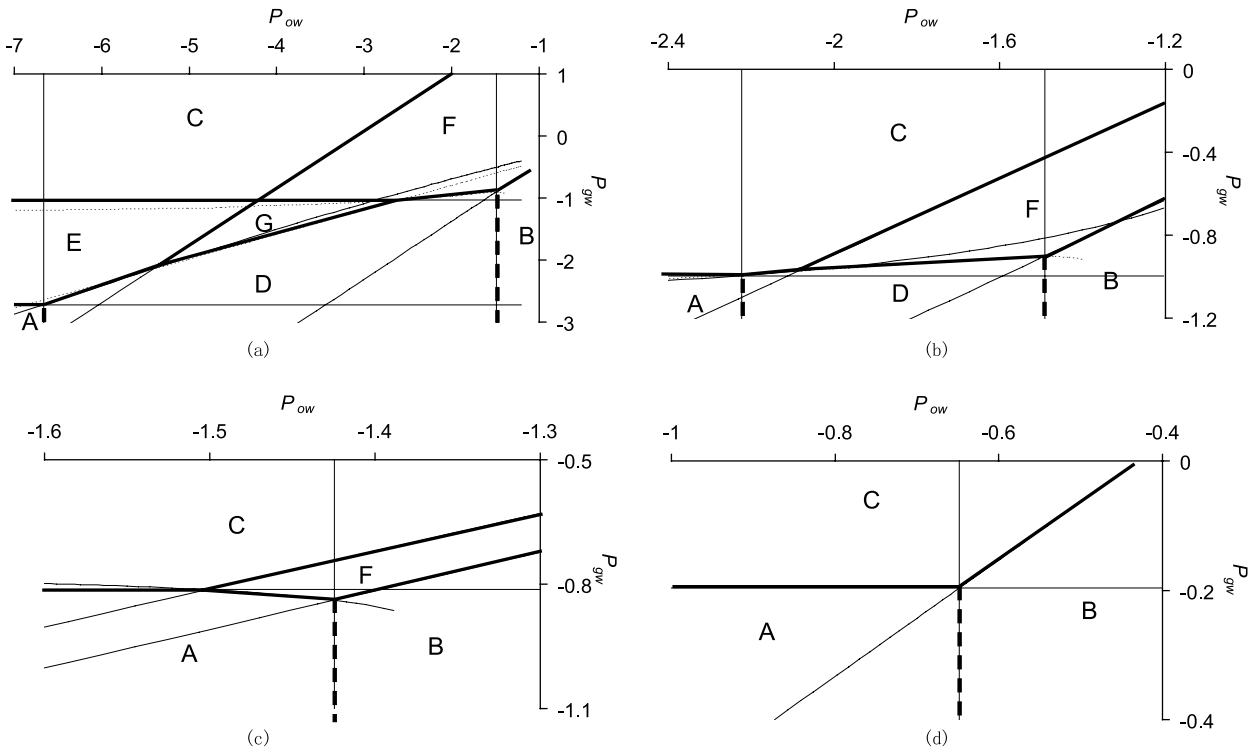

Figure 5. Delineation of the (P_{ow}, P_{gw}) space with respect to the various configurations as presented in Figure 2 using the bold lines for the relevant parts of the displacement criteria for (a) $P_{ow}^{MSP}/P_{ow}^{dr} = 0.1$, (b) $P_{ow}^{MSP}/P_{ow}^{dr} = 0.3$, (c) $P_{ow}^{MSP}/P_{ow}^{dr} = 0.5$, and (d) $P_{ow}^{MSP}/P_{ow}^{dr} = 1.0$.

D → G and G → E, as well as the bulk phase displacement G → F. Comparison with Figure 4a reveals that each of these displacement criteria are stricter than the relevant geometric and snap-off criteria, thereby further reducing the pressure combinations (P_{ow}, P_{gw}) for which configuration G can exist. A similar conclusion can be drawn about the three-phase layer configuration F.

[36] In Figure 5b the delineation of the (P_{ow}, P_{gw}) space is presented for $P_{ow}^{MSP}/P_{ow}^{dr} = 0.3$. In this situation a range of P_{ow} arises where the two-phase oil-water configuration D can still occur. However, in this range the entry pressures for D→E and D→G are now higher than for D→C and D→F, favoring the latter displacements. Comparison of Figures 5a and 5b shows that for low P_{ow}, where essentially only two-phase gas-water configurations can occur (A, C or E), configuration E with gas layers becomes unfavorable when P_{ow}^{dr} decreases, i.e., when a larger portion of the corner becomes water-wet. Furthermore, it may be clear that a necessary condition for the existence of the three-phase configuration G with both gas and oil layers is that both possible two-phase configurations with oil and gas layers, D and E respectively, should be allowed.

[37] In Figure 5c the delineation of the (P_{ow}, P_{gw}) space is presented for $P_{ow}^{MSP}/P_{ow}^{dr} = 0.5$. For this relatively low P_{ow}^{dr} the only possible oil-water configurations are A and B, thus further reducing the number of possible configurations. In particular, for high P_{ow} it is surprising to find that gas invasion still involves configuration F with an oil layer, as opposed to the direct displacement B→C. Furthermore, for low P_{ow} we find that also displacement A→F occurs, contrary to situations with less water in the corners. However, comparison of Figures 5b and 5c reveal that the actual size of the window of (P_{ow}, P_{gw}) in which configuration F can occur has decreased with decreasing P_{ow}^{dr}. Obviously, displacement A→F, in which a bulk gas displacement drags in an oil layer, can only occur in a porous medium if oil is available in neighboring pores.

[38] Finally, in Figure 5d the delineation of the (P_{ow}, P_{gw}) space is presented for $P_{ow}^{MSP}/P_{ow}^{dr} = 1.0$, i.e., when drainage has not proceeded beyond the oil-water entry condition. In this situation the entry pressures for displacements A→C and B→C are lower than those for displacements A→F and B→F respectively, thus excluding configuration F.

4. Conclusions

[39] We have derived the thermodynamic pressure criteria for formation and removal of fluid layers during three-phase flow in an angular pore of nonuniform wettability, embedded in the general theory of deriving three-phase capillary entry pressures for bulk displacements. We have considered the particular case of three-phase gas invasion in a star shaped pore and a particular choice of interfacial tensions and contact angles. The latter have been chosen, such that gas is wetting to water on the surface of altered wettability. This has led to the most complicated combination of pore fluid configurations possible, which makes this case general enough to be extended straightforwardly to other cases.

[40] Conclusions are as follows: 1. The pressure criteria for layer displacements are consistent with the entry pressures for bulk displacements, for the described displacement history, here gas invasion following a water flood. This leads to a unique delineation of the space of

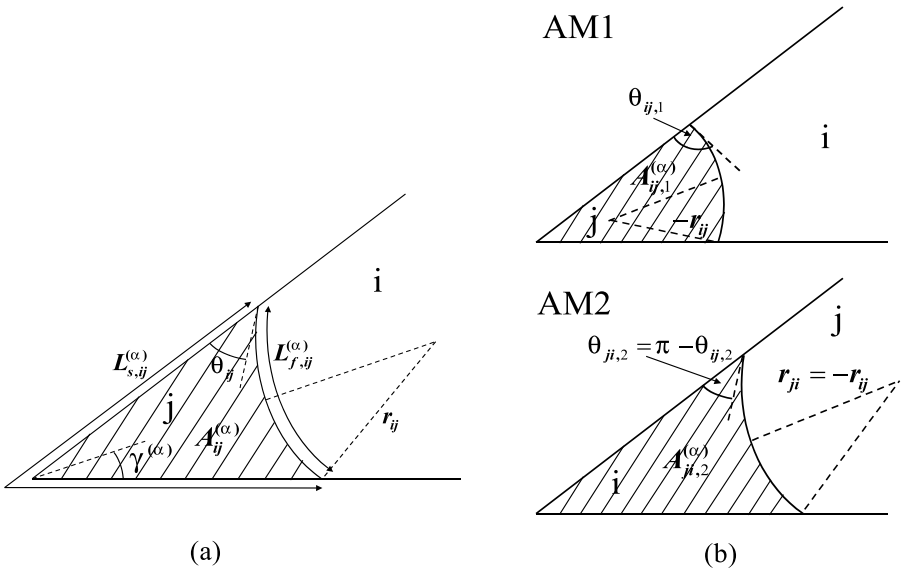

Figure A1. (a) Cross-sectional area $A_{ij}^{(\alpha)}$ occupied by phase j in corner α in the presence of bulk phase i, where the lengths of the surrounding fluid-solid and fluid-fluid contact lines are indicated as $L_{s,ij}^{(\alpha)}$ and $L_{f,ij}^{(\alpha)}$, respectively. (b) Definitions of these areas and the corresponding contact angles for a pinned AM1 with negative curvature and an AM2 with reversed indices.

pressure combinations with respect to the possible fluid configurations. 2. Only for a large drainage pressure, i.e., when the remaining water-wet surface in the pore corners is small, can all possible fluid configurations arise, in particular the configuration in which both a gas and an oil layer occur. 3. The thermodynamic criteria for the existence of layers in three-phase fluid configurations are much more restrictive than existing geometrical criteria. 4. Bulk gas invasion into a water-filled pore may be accompanied by invasion of an oil layer.

[41] Obviously, the full implications of the criteria will become evident after they have been implemented in a pore-scale network model.

Appendix A: Pore Geometry, Geometrical Criteria and Two-Phase Capillary Entry Pressures

[42] For the star-shaped pore cross section of Figure 1 the cross-sectional area and perimeter are given as $A = \frac{3\sqrt{3}}{2}\frac{\sin\left(\frac{\pi}{3}+\gamma\right)}{\sin\gamma}r_{in}^2$ and $L_s = \frac{3\sqrt{3}}{\sin\gamma}r_{in}$, respectively, where r_{in} denotes the inscribed radius. The areas and contact lengths in each corner α are defined as

$$A^{(\alpha)} = r^2\left(\theta + \gamma^{(\alpha)} - \frac{\pi}{2} + \cos\theta\frac{\cos\left(\theta+\gamma^{(\alpha)}\right)}{\sin\gamma^{(\alpha)}}\right) \tag{A1a}$$

$$L_s^{(\alpha)} = 2r\frac{\cos\left(\theta+\gamma^{(\alpha)}\right)}{\sin\gamma^{(\alpha)}} \tag{A1b}$$

$$L_f^{(\alpha)} = 2r\left(\frac{\pi}{2} - \theta - \gamma^{(\alpha)}\right) \tag{A1c}$$

with $A^{(\alpha)}(r_{ij}, \theta_{ij}) = A_{ij}^{(\alpha)}$, $L_s^{(\alpha)}(r_{ij}, \theta_{ij}) = L_{s,ij}^{(\alpha)}$, $L_f^{(\alpha)}(r_{ij}, \theta_{ij}) = L_{f,ij}^{(\alpha)}$, which are explained in Figure A1a. Notice that for the regular star, $\gamma^{(\alpha)} = \gamma$ is the same for all corners. We adopt the convention that θ_{ij} is measured through phase j (second index), while r_{ij} is defined positive when pointing into phase i (first index) and negative when pointing into phase j. The latter is the case for AM 1 in Figure A1b. For example for AM2 in configuration E, Figure A1b explains that

$$L_s^{(\alpha)}\left(r_{wg}, \theta_{wg,2}\right) = 2r_{gw}\frac{\cos\left(\theta_{gw,2}-\gamma\right)}{\sin\gamma} \tag{A2}$$

additionally using that $r_{ji} = -r_{ij}$ and $\theta_{ji} = \pi - \theta_{ij}$.

[43] AM1 can exist only if $\theta_{ij,1} \le \theta_{ij,1}^{sn}$ (see Figure A1b), where $\theta_{ij,1}^{sn}$ denotes the angle at which snap-off of AM1 occurs. $\theta_{ij,1}^{sn} = \theta_{ij,1}^{o}$, where $\theta_{ij,1}^{o}$ is the value of $\theta_{ij,1}$ at the oil-wet surface, or $\theta_{ij,1}^{sn} = \pi - \gamma^{(\alpha)}$ if the latter is smaller than $\theta_{ij,1}^{o}$ [*Blunt*, 1997]. The corresponding snap-off pressure difference P_{ij}^{sn} follows from equations (1) and (5) as

$$P_{ij}^{sn} = \frac{2\sigma_{ij}}{L_s^{dr}}\frac{\cos\left(\theta_{ij,1}^{sn}+\gamma\right)}{\sin\gamma}, \tag{A3}$$

where AM1 does exist only if $P_{ij} \ge P_{ij}^{sn}$.

[44] AM2 can exist only if $\theta_{ij,2} \le (\pi/2) - \gamma$, where we use the ordering of indices as in Figure A1a. Furthermore, the corresponding radius of curvature r_{ij} must be smaller than r_{in}, which is the equivalent to $L_s^{(\alpha)} = L_s/3$ for the three-cornered star. The corresponding pressure difference follows from equation (A1b) as

$$P_{ij}^{sn} = \frac{2\sigma_{ij}}{r_{in}}\frac{\cos\left(\theta_{ij,2}+\gamma\right)}{\sqrt{3}}. \tag{A4}$$

where AM2 exists only if $P_{ij} \le P_{ij}^{sn}$.

[45] In addition to the snap-off criteria, which apply to individual AMs, geometric criteria for the existence of the layers apply. The two-phase gas or oil layer between water and water, present in configurations C and D, respectively, can exist only if the surrounding AMs do not touch. The corresponding geometrical layer collapse pressure difference P_{iw}^{geom} follows from equations (5) and (A1b), using some elementary trigonometry [*Øren et al.*, 1998] as

$$P_{iw}^{geom} = \frac{2\sigma_{iw}\cos\left(\theta_{iw,h}+\gamma\right)}{L_s^{dr}\sin\gamma}, \tag{A5}$$

where $\cos\theta_{iw,h} = \cos\left(\tilde{\theta}_{iw}+\gamma\right) + 2\sin\gamma$ for $i = g, o$, with $\tilde{\theta}_{ow} = \theta_{ow,a}^{o}$ and $\tilde{\theta}_{gw} = \theta_{gw,r}^{o}$. The layer exists only if $P_{iw} \geq P_{iw}^{geom}$.

[46] The geometrical criterion for the oil layer between gas and water, present in configurations F and G, can be formulated in terms of a gas-water pressure difference P_{gw}^{geom} as a function of P_{ow} (assuming that the AMs touch at their centers, since $\theta_{go,r}^{o} < \theta_{ow,h}$) [*Hui and Blunt*, 2000; *Piri and Blunt*, 2004] as

$$P_{gw}^{geom} = P_{ow}\left(\frac{\sigma_{go}}{\sigma_{ow}}\left(\frac{\cos\theta_{go,r}^{o}-\sin\gamma}{\cos\theta_{ow,h}-\sin\gamma}\right)+1\right), \tag{A6}$$

where

$$\cos\left(\theta_{ow,h}+\gamma\right) = \frac{P_{ow}}{\sigma_{ow}}\frac{L_s^{dr}}{2}\sin\gamma.$$

The layer exists only if $P_{gw} \leq P_{gw}^{geom}$. The geometrical criterion for the gas layer between water and oil, present in configuration G (assuming that the AMs touch at the pore walls, since $\theta_{go,r}^{o} < \pi - \theta_{gw,r}^{o}$) [*Fenwick and Blunt*, 1998] is given by

$$P_{gw}^{geom} = P_{ow}\Big/\left[1-\frac{\sigma_{go}}{\sigma_{gw}}\frac{\cos\left(\theta_{go,r}^{o}+\gamma\right)}{\cos\left(\theta_{gw,r}^{o}-\gamma\right)}\right]. \tag{A7}$$

The layer exists only if $P_{gw} \geq P_{gw}^{geom}$.

[47] For completeness we also give the "classical" analytical solution of the equation $dF = 0$ for a two-phase displacement. For a general two-phase displacement, equation (2) reduces to

$$dF = P_{ij}dV_j + \sigma_{ij}\left(dA_{ij} - \cos\theta_{ij}^{MTM}dA_{js}\right) \tag{A8}$$

with $i, j = g, o, w$ and $i \neq j$. The classical solution can be found when the same (nonhinging) contact angle θ_{ij} arises at the MTM and at the single (relevant) AM in each corner, such as during primary drainage or for example for displacement G→F. For the three-cornered star this solution is given as the method of standard porosimetry capillary entry pressure

$$P_{ij}^{MSP} = \frac{\sigma_{ij}}{r_{in}}\frac{\cos\theta_{ij}+\sqrt{\cos^2\theta_{ij}-\frac{2}{\sqrt{3}}\sin\left(\frac{\pi}{3}+\gamma\right)\sin\gamma\left(\theta_{ij}+\gamma-\frac{\pi}{2}+\cos\theta_{ij}\frac{\cos\left(\theta_{ij}+\gamma\right)}{\sin\gamma}\right)}}{\sin\left(\frac{\pi}{3}+\gamma\right)} \tag{A9}$$

This expression reduces to that for an equilateral triangle when $\gamma = \pi/6$ [e.g., *Ma et al.*, 1996; *Lago and Araujo*, 2001].

[48] **Acknowledgments.** M. I. J. van Dijke and K. S. Sorbie acknowledge funding from EPSRC under grant EP/D002435/1. M. Piri wishes to thank EORI of University of Wyoming for its support. Support for J. O. Helland was provided by Statoil through the VISTA program.

References

Blunt, M. J. (1997), Pore level modeling of the effects of wettability, *SPE J.*, *2*, 494–510.

DiCarlo, D. A., A. Sahni, and M. J. Blunt (2000), Three-phase relative permeability of water-wet, oil-wet and mixed-wet sandpacks, *SPE J.*, *5*, 82–91.

Dong, M., and I. Chatzis (2003), Oil layer flow along the corners of non-circular capillaries by gravity drainage, *J. Can. Pet. Technol.*, *42*, 9–11.

Dong, M., F. A. L. Dullien, and I. Chatzis (1995), Imbibition of oil in film form over water present in edges of capillaries with an angular cross-section, *J. Colloid Interface Sci.*, *172*, 278–288.

Fenwick, D. H., and M. J. Blunt (1998), Three-dimensional modeling of three phase imbibition and drainage, *Adv. Water Resour.*, *21*, 121–143.

Firoozabadi, A. (1999), *Thermodynamics of Hydrocarbon Reservoirs*, McGraw-Hill, New York.

Grattoni, C. A., M. B. Pingo Almada, and R. A. Dawe (1997), Pore and core-scale displacement mechanisms with spreading and wetting effects during three-phase flow, paper SPE 39032 presented at Latin American and Caribbean Petroleum Engineering Conference, Soc. of Pet. Eng., Rio de Janeiro, Brazil, Aug.

Helland, J. O., and S. M. Skjæveland (2006), Three-phase mixed-wet capillary pressure curves from a bundle-of-triangular-tubes model, *J. Pet. Sci. Eng.*, *52*, 100–130, doi:10.1016/j.petrol.2006.03.018.

Hui, M.-H., and M. J. Blunt (2000), Effects of wettability on three-phase flow in porous media, *J. Phys. Chem. B*, *104*, 3833–3845.

Keller, A. A., M. J. Blunt, and P. V. Roberts (1997), Micromodel observation of the role of oil layers in three-phase flow, *Transp. Porous Media*, *26*, 277–297.

Kovscek, A. R., H. Wong, and C. J. Radke (1993), A pore-level scenario for the development of mixed wettability in oil reservoirs, *AIChE J.*, *39*, 1072–1085.

Lago, M., and M. Araujo (2001), Threshold pressure in capillaries with polygonal cross section, *J. Colloid Interface Sci.*, *243*, 219–226, doi:10.1006/jcis.2001.7872.

Lerdahl, T. R., P. E. Øren, and S. Bakke (2000), A predictive network model for three-phase flow in porous media, paper SPE59311 presented at SPE/DOE Conference on Improved Oil Recovery, Soc. of Pet. Eng., Tulsa, Okla., April.

Ma, S., G. Mason, and N. R. Morrow (1996), Effect of contact angle on drainage and imbibition in regular polygonal tubes, *Colloids Surf. A*, *117*, 273–291.

Mayer, R. P., and R. A. Stowe (1965), Mercury porosimetry–breakthrough pressure for penetration between packed spheres, *J. Colloid Interface Sci.*, *20*, 893–911.

Øren, P. E., J. Billiotte, and W. V. Pinczewski (1992), Mobilization of waterflood residual oil by gas injection for water-wet conditions, *SPE Form. Eval.*, *7*, 70–78.

Øren, P. E., S. Bakke, and O. J. Arntzen (1998), Extending predictive capabilities to network models, *SPE J.*, *3*, 324–336.

Patzek, T. W. (2001), Verification of a complete pore network simulator of drainage and imbibition, *SPE J.*, *6*, 144–156.

Piri, M., and M. J. Blunt (2004), Three-phase threshold capillary pressures in noncircular capillary tubes with different wettabilities including con-

tact angle hysteresis, *Phys. Rev. E.*, *70*, 061603, doi:10.1103/PhysRevE.70.061603.

Piri, M., and M. J. Blunt (2005a), Three-dimensional mixed-wet random pore-scale network modeling of two- and three-phase flow in porous media. I. Model description, *Phys. Rev. E*, *71*, 026301, doi:10.1103/PhysRevE.71.026301.

Piri, M., and M. J. Blunt (2005b), Three-dimensional mixed-wet random pore-scale network modeling of two- and three-phase flow in porous media. II. Results, *Phys. Rev. E*, *71*, 026302, doi:10.1103/PhysRevE.71.026302.

Princen, H. M. (1969a), Capillary phenomena in assemblies of parallel cylinders. I. Capillary rise between two cylinders, *J. Colloid Interface Sci.*, *30*, 69–75.

Princen, H. M. (1969b), Capillary phenomena in assemblies of parallel cylinders. II. Capillary rise in systems with more than two cylinders, *J. Colloid Interface Sci.*, *30*, 359–371.

Princen, H. M. (1970), Capillary phenomena in assemblies of parallel cylinders. III. Liquid columns between horizontal parallel cylinders, *J. Colloid Interface Sci.*, *34*, 171–184.

Sahni, A., J. Burger, and M. J. Blunt (1998), Measurement of three phase relative permeability during gravity drainage using CT scanning, paper SPE39655 presented at SPE/DOE Improved Oil Recovery Symposium, Soc. of Pet. Eng., Tulsa, Okla., April .

Sohrabi, M., D. H. Tehrani, A. Danesh, and G. D. Henderson (2004), Visualization of oil recovery by water-alternating-gas injection using high-pressure micromodels, *SPE J.*, *9*, 290–301.

Valvatne, P. H., and M. J. Blunt (2004), Predictive pore-scale modeling of two-phase flow in mixed wet media, *Water Resour. Res.*, *40*, W07406, doi:10.1029/2003WR002627.

van Dijke, M. I. J., and K. S. Sorbie (2003), Three-phase capillary entry conditions in pores of non-circular cross-section, *J. Colloid Interface Sci.*, *260*, 385–397, doi:10.1016/S0021-9797(02)00228-X.

van Dijke, M. I. J., and K. S. Sorbie (2006), Existence of fluid layers in the corners of a capillary with non-uniform wettability, *J. Colloid Interface Sci.*, *293*, 455–463, doi:10.1016/j.jcis.2005.06.059.

van Dijke, M. I. J., and K. S. Sorbie (2007), Consistency of three-phase capillary entry pressures and pore phase occupancies, *Adv. Water Resour.*, *30*, 182–198, doi:10.1016/j.advwatres.2005.03.024.

van Dijke, M. I. J., M. Lago, K. S. Sorbie, and M. Araujo (2004), Free energy balance for three fluid phases in a capillary of arbitrarily shaped cross-section: Capillary entry pressures and layers of the intermediate-wetting phase, *J. Colloid Interface Sci.*, *277*, 184–201, doi:10.1016/j.jcis.2004.05.021.

M. J. Blunt, Department of Earth Science and Engineering, Imperial College, London SW7 2AZ, UK.

J. O. Helland, International Research Institute of Stavanger, PO Box 8046, N-4068 Stavanger, Norway.

M. Piri, Department of Chemical and Petroleum Engineering, University of Wyoming, Laramie, WY 82071-2000, USA.

S. M. Skjæveland, Department of Petroleum Engineering, University of Stavanger, N-4036 Stavanger, Norway.

K. S. Sorbie and M. I. J. van Dijke, Institute of Petroleum Engineering, Heriot-Watt University, Edinburgh EH14 4AS, UK. (rink@pet.hw.ac.uk)